

# Data reduction and processing for photon science detectors

David Pennicard<sup>1,\*</sup>, Vahid Rahmani<sup>1</sup> and Heinz Graafsma<sup>1,2</sup>

<sup>1</sup>*Deutsches Elektronen-Synchrotron DESY, Notkestr. 85, 22607 Hamburg, Germany*

<sup>2</sup>*Mid Sweden University, Sundsvall, Sweden*

Correspondence\*:

Corresponding Author

david.pennicard@desy.de

## 2 ABSTRACT

3 New detectors in photon science experiments produce rapidly-growing volumes of data. For  
4 detector developers, this poses two challenges; firstly, raw data streams from detectors must be  
5 converted to meaningful images at ever-higher rates, and secondly, there is an increasing need  
6 for data reduction relatively early in the data processing chain. An overview of data correction  
7 and reduction is presented, with an emphasis on how different data reduction methods apply  
8 to different experiments in photon science. These methods can be implemented in different  
9 hardware (e.g. CPU, GPU or FPGA) and in different stages of a detector's data acquisition (DAQ)  
10 chain; the strengths and weaknesses of these different approaches are discussed.

11 **Keywords:** Photon science, detectors, X-rays, data processing, data reduction, hardware acceleration, DAQ

## 1 INTRODUCTION

12 Developments in photon science sources and detectors have led to rapidly-growing data rates and volumes  
13 [1]. For example, experiments at the recently-upgraded ESRF EBS can potentially produce a total of a  
14 petabyte of data per day, and future detectors targeting frame rates over 100 kHz will have data rates (for  
15 raw data) exceeding 1 Tbit/s [2].

16 These improvements not only allow a much higher throughput of experiments, but also make new  
17 measurements feasible. For example, by focusing the beam and raster-scanning it across a sample at  
18 high speed, essentially any X-ray technique can be used as a form of microscopy, obtaining atomic-scale  
19 structure and chemical information about large samples. But naturally, these increasing data rates pose  
20 a variety of challenges for data storage and analysis. In particular, there is increasing demand for data  
21 reduction, to ensure that the volume of data that needs to be transferred and stored is not unfeasibly large.  
22 From the perspective of detector developers, there are two key issues that need to be addressed.

23 Firstly, the raw data stream from a detector needs to be converted into meaningful images, as discussed  
24 in section 2, and this becomes increasingly challenging at high data rates. This conversion process is  
25 detector-specific, so implementing it requires detailed knowledge of the detector's characteristics. At the  
26 same time, since the correction process is relatively fixed, there's a lot of potential to use accelerators  
27 such as GPUs or FPGAs to do this. In addition, the complexity of this conversion process depends on the  
28 detector design, so this is something that should be considered during detector development.

Secondly, it can be beneficial to perform data reduction on-detector, or as part of the detector's DAQ system. For a variety of reasons, the useful information in a dataset can be captured with a smaller number of bits than the original raw data size; for example, by taking advantage of patterns or redundancy in the raw data, or by rejecting non-useful images in the dataset. In the DAQ system, the data will typically pass through a series of stages, as illustrated in Fig. 1 - firstly, from the ASIC or monolithic sensor to a custom board in the detector, then to a specialized DAQ PC (or similar hardware), and finally to a more conventional computing environment. By performing data reduction early on in this chain, it is possible to reduce the bandwidth required by later stages. Not only can this reduce the cost and complexity of later stages, it can also potentially enable the development of faster detectors by overcoming data bandwidth bottlenecks. Performing this early data reduction often ties together with the process of converting the raw data stream to real images, since these can be easier to compress. Conversely, though, performing data reduction early in the chain can be more challenging, since the hardware in these early stages tends to offer less flexibility, and there are constraints on space and power consumption within the detector.

This paper presents an overview of image correction and data reduction in photon science, with a particular focus on how the characteristics of different detectors and experiments affect the choice of data reduction algorithm. After a discussion of the features of common data processing hardware - CPUs, GPUs and FPGAs - the paper returns to the topic of how different compression methods may be implemented in different stages of a detector's data acquisition chain.

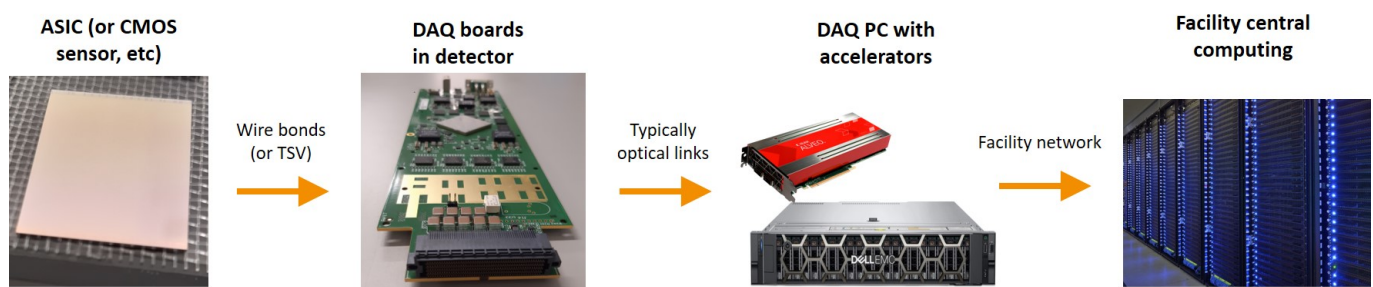


**Figure 1.** Illustration of typical elements in a detector's DAQ chain.

## 2 DETECTOR DATA CORRECTION

The raw data stream produced by a detector generally requires processing in order to produce a meaningful image. The steps will of course depend on the design; here, two common cases of photon counting and integrating pixel detectors are considered. Although it can be possible to compress data before all corrections are applied, corrected data can be more compressible - for example, correcting pixel-to-pixel variations can result in a more uniform image.

Firstly, we want the pixels in an image to follow a straightforward ordering; typically this is row-by-row or column-by-column, though some image formats represent images as a series of blocks for performance reasons. However, data streams from detectors often have a more complex ordering. One reason for this is that data readout from an ASIC or monolithic detector is typically parallelized across multiple readout signal lines which can result in interleaving of data. In addition, in detectors composed of multiple chips or modules, there may be gaps in the image, or some parts of the detector may be rotated - this is illustrated for the AGIPD 1M detector [3] in Fig 2. So, data reordering is a common first step.

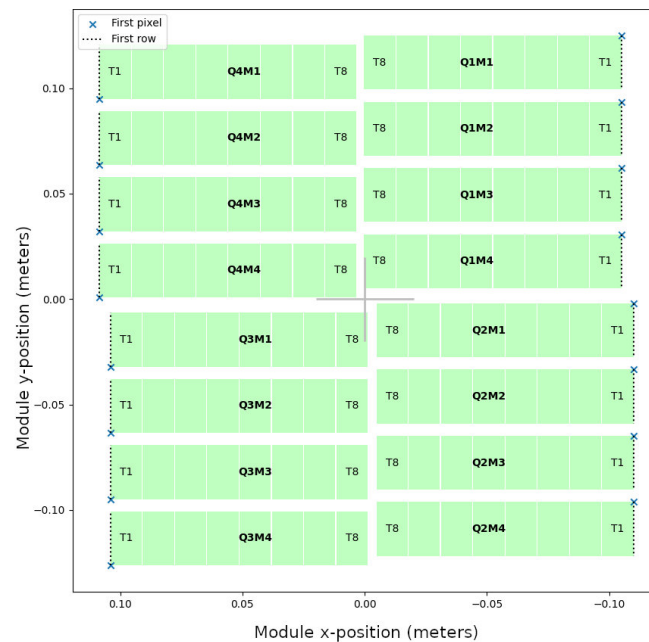


**Figure 2.** Module layout of the AGIPD 1M detector, which has a central hole for the beam, gaps between modules, and different module orientations (with the first pixel of each module indicated by a cross).

59 In the case of photon counting detectors, the value read out from each pixel correspond relatively directly  
 60 to the number of photons hitting the pixel. Nevertheless, at higher count rates losses occur due pulse  
 61 pileup, when photons hit a pixel in quick succession. So, pileup correction is needed. Although there are  
 62 two well-known models for pileup - paralyzable and non-paralyzable - in practice the behaviour of pixel  
 63 detectors can be somewhere in-between, and in addition to this some modern detectors have additional  
 64 pileup compensation, for example by detecting longer pulses that would indicate pileup [4] . So, the pileup  
 65 correction process can vary between different detectors.

66 In integrating detectors, each pixel's amplifier produces an analog value, which is then digitized. This  
 67 digitized value then needs to be converted to the energy deposited in the pixel. In many detectors, this is  
 68 a linear relationship which can be described in terms of a baseline and gain; these parameters can vary  
 69 from pixel-to-pixel. As discussed later, if the incoming X-ray beam is monochromatic then the measured  
 70 energy may then be converted to photons. In some integrating detectors designed for large dynamic range,  
 71 the response may not be a simple linear one. For example, in dynamic gain switching detectors [3] each  
 72 pixel can adjust its gain in response to the magnitude of the incoming signal, and the output of each pixel  
 73 consists of a digitized value plus information on which gain setting was used; for each gain setting, there is  
 74 a different baseline and gain that need to be applied to calculate the energy deposited in the pixel.

75 In practice, detectors may deviate from the ideal response, and additional corrections may be required.  
 76 For example, the response of a detector may not be fully linear, and more complex functions may be need  
 77 to describe their response. There may also be phenomena such as common-mode signals or crosstalk,  
 78 where corrections need to be applied that are dependent on the magnitude and pattern of the incoming  
 79 signal rather than independent for each pixel. It is also common to treat malfunctioning pixels, for example  
 80 by setting them to some special value.

81 An additional aspect of detector data processing is combining the image data with metadata. Some  
82 metadata may be directly incorporated into the detector's data stream. For example, in Free Electron Laser  
83 (FEL) experiments the detector needs to be synchronised with the X-ray bunches, and bunches can vary in  
84 quality, so each image will be accompanied by a bunch ID, fed to the detector from the facility's control  
85 system. Other metadata may be added later. For example, the NeXuS data format [5] has been adopted  
86 by many labs; this is based on the HDF5 format [6], and specifies how metadata should be structured in  
87 experiments in photon science and other fields.

### 3 DATA COMPRESSION AND PHOTON SCIENCE DATASETS

88 In general, data compression algorithms reduce the number of bits needed to represent data, by encoding it  
89 in a way that takes advantage of patterns or redundancy in the data. These algorithms can be subdivided  
90 into lossless compression [7], where the original data can be reconstructed with no error, and lossy  
91 compression [8], where there is some difference between the original and reconstructed data. Currently,  
92 lossless compression is often applied to photon science data before storage, whereas lossy compression  
93 is uncommon, due to concerns about degrading or biasing the results of later analysis. However, lossy  
94 compression can achieve higher compression ratios.

95 The compressibility of an image naturally depends on its content, and in photon science this can vary  
96 depending on both the type of experiment and the detector characteristics. In particular, since random  
97 noise will not have any particular redundancy or pattern, the presence of noise in an image will reduce the  
98 amount of compression that can be achieved with lossless algorithms.

99 Compared to typical visible light images, X-ray images from pixel detectors can have distinctive features  
100 that affect their compressibility, as discussed further below. Firstly, individual X-ray photons have much  
101 greater energy and thus can more easily be discriminated with a suitable detector. Also, X-ray diffraction  
102 patterns have characteristics that can make lossless compression relatively efficient. However, imaging  
103 experiments using scintillators and visible light cameras produce images more akin to conventional visible  
104 light imaging, which do not losslessly compress well.

#### 105 3.1 Noise in X-ray images, and its effects on compression

106 Random noise in an image can potentially come from different sources; firstly, electronic noise introduced  
107 by the detector, and secondly, inherent statistical variation in the experiment itself.

108 Any readout electronics will inevitably have electronic noise. However, the signal seen by a detector  
109 consists of discrete X-ray photons, and the inherent discreteness of our signal makes it possible to reject  
110 the electronic noise, provided that it is small compared to the signal produced by a single photon. In a  
111 silicon sensor without gain, we will generate on average one electron-hole pair per 3.6 eV of energy, e.g. a  
112 12 keV photon will generate approximately 3300 electrons. In turn, if for example the electronic noise is  
113 Gaussian with a standard deviation corresponding to 0.1 times the photon energy (330 electrons here) then  
114 the probability of a pixel having a noise fluctuation corresponding to 0.5 photons or more is approximately  
115 1 in 1.7 million [9].

116 In integrating pixel detectors, each pixel measures the total energy deposited in the pixel during the  
117 integration time of the image. If the photon source is monochromatic, then it is possible to convert the  
118 integrated signal to an equivalent number of photons in postprocessing. Given sufficiently low noise,  
119 this value can be quantized to the nearest whole number of photons to eliminate electronic noise. In  
120 photon counting detectors, a hit will be recorded in a pixel if the pulse produced by the photon exceeds



121 a user-defined threshold; once again, if the threshold level is far enough from the noise, we will have  
 122 effectively noise-free counting.

123 In both cases, the electronic noise in a pixel will be dependent on the integration time for an image, or  
 124 the shaping time in the case of a photon-counting detector. There are two main competing effects here.  
 125 On the one hand, for longer timescales, the shot noise due to fluctuations in leakage current will be larger.  
 126 Conversely, to achieve shorter integration times or shaping times, a higher amplifier bandwidth is required,  
 127 and this will increase the amount of thermal noise detected [10]. Thermal noise is the noise associated with  
 128 random thermal motion of electrons, which is effectively white noise.

129 In addition to electronic noise, however, the physics of photon emission and interaction are inherently  
 130 probabilistic, and so even if an experiment were repeated under identical conditions there would be  
 131 statistical fluctuations in the number of photons impinging on each pixel. These fluctuations follow Poisson  
 132 statistics, and if the expected number of photons arriving in a pixel during a measurement is  $N$ , then the  
 133 standard deviation of the corresponding Poisson distribution will be  $\sqrt{N}$ . On the one hand, this can  
 134 make it easier to develop "low noise" detectors; provided the detector noise for a given photon flux is  
 135 significantly smaller than  $\sqrt{N}$ , then it will have little effect on the final result. However, this makes  
 136 the data less compressible with lossless algorithms, since random noise introduces variation in the image  
 137 that is not patterned or redundant. (As discussed later, quantizing pixel values with a variable step size,  
 138 increasing with  $\sqrt{N}$ , can be a way of achieving lossy compression.)

### 139 3.2 Applying lossless compression to diffraction data

140 As noted above, data compression relies on patterns or redundancy in data, and this will vary depending  
 141 on the experiment. Diffraction patterns differ from conventional images in a variety of respects, with the  
 142 pattern being mathematically related to the Fourier transform of the object. An example of a diffraction  
 143 pattern from macromolecular crystallography is shown in Fig. 3.

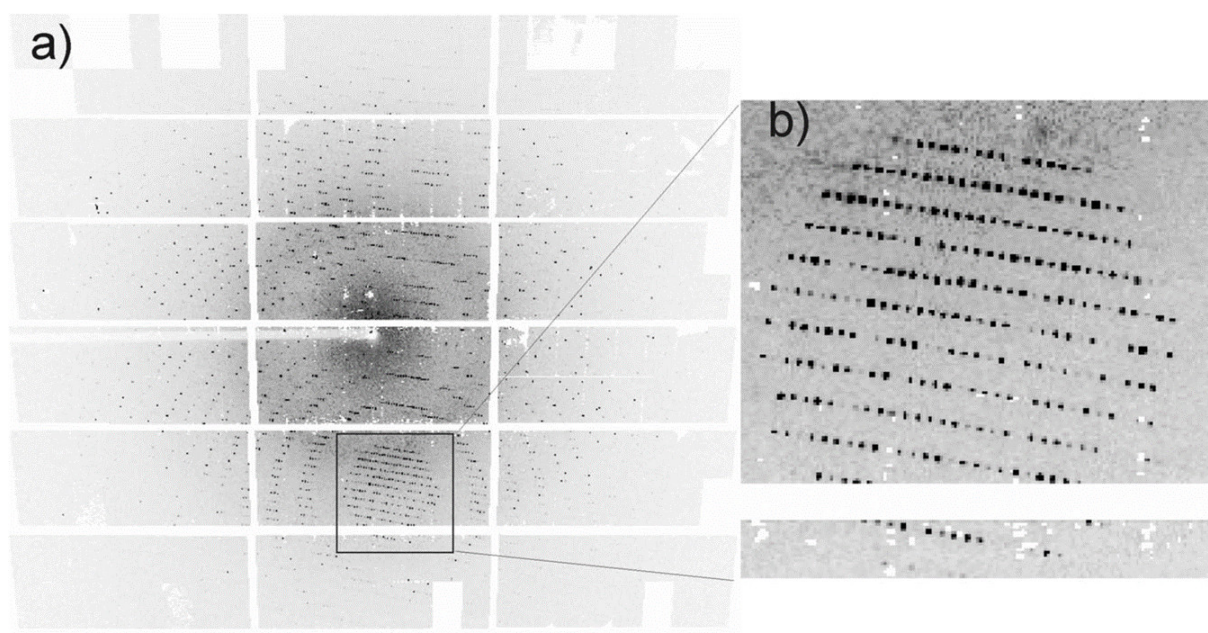


**Figure 3.** A diffraction pattern from a thaumatin crystal, recorded with a Pilatus 1M detector. Reproduced from [11] with permission of the International Union of Crystallography.

144 Diffraction patterns tend to have various features that are advantageous for lossless compression:

- 145 • Hybrid pixel detectors with sensitivity to single photons are the technology of choice for these  
146 experiments, making the measurement effectively free from electronic noise as described above.  
147 (Detectors for X-ray diffraction require high sensitivity, but pixel sizes in the range of 50-200  $\mu\text{m}$  are  
148 generally acceptable.)
- 149 • The intensity values measured in the detector typically have a nonuniform distribution, with most  
150 pixels measuring relatively low or even zero photons, and a small proportion of pixels having higher  
151 values. This is partly because the diffracted intensity drops rapidly at higher scattering angles, and  
152 partly because of interference phenomena that tend to produce high intensity in certain places (e.g.  
153 Bragg spots or speckles) and low intensity elsewhere.
- 154 • As with many images, nearby pixels will tend to have similar intensities.
- 155 • Combining these points, in images with fewer photons, there can be patches in the image with many  
156 neighbouring zero-value pixels.

157 Empirically, a range of lossless compression algorithms can achieve good results with diffraction data,  
158 especially in high-frame-rate measurements where the number of photons per image will tend to be  
159 lower. Experiments applying the DEFLATE [12] algorithm used in GZIP to datasets acquired with photon  
160 counting detectors running at high speed showed compression ratios of 19 for high-energy X-ray diffraction,  
161 70 for ptychography and 350 for XPCS experiments with dilute samples (where most pixel values are zero)  
162 [13]. Experiments with the Jungfrau integrating detector, applying different compression algorithms to the  
163 same data, found that multiple compression methods such as GZIP, LZ4 with a bitshuffle filter and Zstd  
164 gave similar compression ratios to one another, but varied greatly in speed, with GZIP being a factor of 10  
165 slower [14].

### 166 3.2.1 Example - lossless compression with DEFLATE (GZIP) and Bitshuffle/LZ4

167 As illustrative examples, we consider the DEFLATE algorithm used in GZIP [15], and the Bitshuffle/LZ4  
168 algorithm [16], firstly to discuss how they take advantage of redundancy to compress diffraction data, and  
169 secondly how algorithms with different computational cost can achieve similar performance.

170 DEFLATE [12] consists of two stages. Firstly, the LZ77 algorithm [17] is applied to the data, which  
171 searches for recurring sequences of characters in a file (such as repeated words or phrases in text, or  
172 long runs of the same character) and encodes them efficiently. In the output of this algorithm, the first  
173 instance of a sequence of characters is written in full, but then later instances are replaced with special  
174 codes referring back to the previous instance. In diffraction datasets, long recurring sequences of characters  
175 are generally rare, but there is one big exception; long runs of zeroes. So, the pattern-matching in LZ77  
176 will efficiently compress long runs of zeroes, but the computational work the algorithm does to find more  
177 complex recurring sequences is largely wasted.

178 Secondly, DEFLATE takes the output of the LZ77 stage, and applies Huffman coding [18] to it. Normally,  
179 different characters in a dataset (e.g. integers in image data) are all represented with the same number  
180 of bits. Huffman coding looks at the frequencies of different characters in the dataset, and produces a  
181 new coding scheme that represents common characters with shorter sequences of bits and rare ones with  
182 longer sequences. This is analogous to Morse code, where the most common letter in English, "E", is  
183 represented by a single dot, whereas rare letters have longer sequences. For diffraction data, this stage will  
184 achieve compression due to the nonuniform statistics of pixel values, where low pixel values are much  
185 more common than high ones.

As a contrasting example, the Bitshuffle LZ4 algorithm [16] implicitly takes advantage of the knowledge that the higher bits of pixel values are mostly zero and strongly correlated between neighbouring pixels. In the first step, Bitshuffle, the bits in the data stream are rearranged so that the first bit from every pixel are all grouped together, then the second bit, etc. After this regrouping, the result will often contain long runs of bytes with value zero, as illustrated in Fig. 4. The LZ4 algorithm, which is similar to LZ77, will then efficiently encode these long runs of zero bytes. As mentioned above, this algorithm gives similar performance to GZIP for X-ray diffraction data while being less computationally expensive.

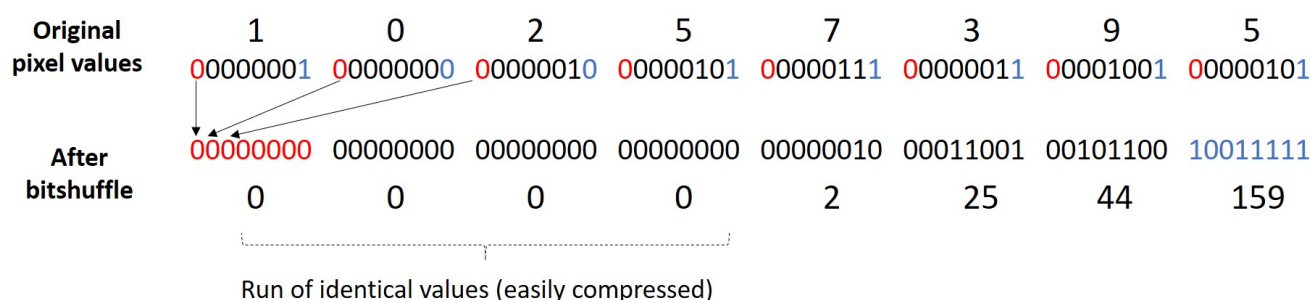


**Figure 4.** Illustration of the Bitshuffle process, used in Bitshuffle/LZ4. This reorders the bits in the data stream so that the LZ4 compression stage can take advantage of the fact that the upper bits in diffraction data are mostly zero, and strongly correlated between neighbouring pixels.

### 3.3 Applying lossy compression to imaging data

While lossless compression can achieve good compression ratios for diffraction data, there is increasing demand for lossy data compression. Firstly, data from some experiments such as imaging do not losslessly compress well, due to noise, and secondly, the increasing data volumes produced by new detectors and experiments mean that higher compression ratios are desirable. The key challenge of lossy compression is ensuring that the compression does not significantly change the final result of analysis. This requires evaluating the results of the compression with a variety of datasets, either by directly comparing the compressed and uncompressed images with a metric of similarity, or by performing the data analysis and applying some appropriate metric of quality to the final result.

In X-ray imaging and tomography experiments, the detector measures X-ray transmission through the sample, and perhaps also additional effects such as enhancement of edges through phase contrast. This means that most pixels will receive a reasonably high X-ray flux, in contrast to X-ray diffraction where most pixels see few or even zero photons. So, noise due to Poisson statistics will be relatively high in most pixels. Likewise, a key requirement for detectors in these experiments is a small effective pixel size, whereas single photon sensitivity is less critical. To achieve this, the typical approach is to couple a thin scintillator to a visible light camera with small pixels such as a CMOS sensor, using magnifying optics [19]. This means that the detector noise is also non-negligible.

Since an X-ray transmission image is a real-space image of an object, and broadly resembles a conventional photograph (unlike a diffraction pattern), widely-used lossy compression algorithms for images can potentially be used for compression. In particular, JPEG2000 [20] is already widely used in medical imaging, and in tomography at synchrotrons it has been demonstrated to achieve a factor of 3-4 compression without significantly affecting the results of the reconstruction [21]. To test this, the reconstruction of the object was performed both before and after compression, and the two results compared

216 using the Mean Structural Similarity Index Measure (MSSIM) metric. A compression factor of 6-8 was  
217 possible in data with a high signal-to-noise ratio.

### 218 3.3.1 Example - lossy compression with JPEG2000

219 One common approach to both lossy and lossless compression is apply a transform to the data that  
220 results in a sparse representation, i.e. most of the resulting values are low or zero. (The choice of transform  
221 naturally depends on the characteristics of the data.) The sparse representation can then be compressed  
222 efficiently.

223 In the case of JPEG2000 [20], the Discrete Wavelet Transform [22] is used; in effect, this transformation  
224 represents the image of a sum of wave packets with different positions and spatial frequencies. This tends  
225 to work well for real space images, which tend to consist of a combination of localized objects and smooth  
226 gradients, which can be found on different length scales. After applying the transform, the resulting values  
227 are typically rounded off to some level of accuracy, allowing for varying degrees of lossy compression.  
228 (By not applying this rounding, lossless compression is also possible.) Then, these values are encoded by  
229 a method called arithmetic coding, which is comparable to Huffman coding; it achieves compression by  
230 taking advantage of the nonuniform statistics of the transformed values, which in this case are mostly small  
231 or zero.

232 JPEG2000 can be compared with the older JPEG standard, where the transformation consists of splitting  
233 the image into  $8 \times 8$  blocks, and applying the Discrete Cosine Transform to each block, thus taking advantage  
234 of the fact that images tend to be locally smooth. This is computationally cheaper than JPEG2000, but one  
235 key drawback is that this can lead to discontinuities between these  $8 \times 8$  blocks after compression.

## 236 3.4 Novel methods for lossy compression

237 As mentioned previously, increasing data volumes mean there is demand for achieving increasing  
238 compression, even for experiments such as X-ray diffraction where lossless compression works reasonably  
239 well. Naturally, this can be approached by testing a variety of well-established lossy compression algorithms  
240 on data, and experimenting with methods such as rounding the data to some level of accuracy. However,  
241 there are also new lossy compression methods being developed specifically for scientific data. One particular  
242 point of contrast is that most image compression algorithms focus on minimizing the perceptible difference  
243 to a human viewer, whereas for scientific data other criteria can be more important, such as imposing limits  
244 on the maximum error allowed between original values and compressed values.

245 One simple example is quantizing X-ray data with a step size smaller than the Poisson noise, which  
246 is proportional to  $\sqrt{(N)}$ . For ptychography, for example, it has been demonstrated that quantizing pixel  
247 values with a step size of  $0.5 \times \sqrt{(N)}$  [23] does not degrade the quality of the reconstruction.

248 A more sophisticated example of error-bounded lossy compression is the SZ algorithm [24], which is a  
249 method for compressing a series of floating-point values. For each new element in the series, the algorithm  
250 checks if its value can be successfully "predicted" (within a specified margin of error) using any one of  
251 three methods: directly taking the previous value; linear extrapolation from the previous two values; or  
252 quadratically extrapolating from the previous three values. If so, then the pixel value is represented by a  
253 2-bit code indicating the appropriate prediction method. If not, then this "unpredictable" value needs to be  
254 stored explicitly. This is illustrated in Fig. 5. After the algorithm runs, further compression is applied to the  
255 list of unpredictable values.



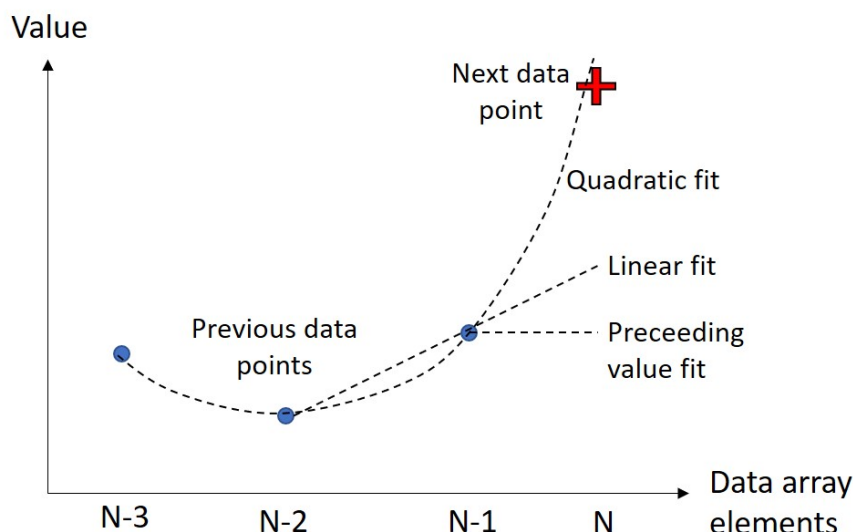


**Figure 5.** Illustration of the "predictive" approach used in SZ compression of floating-point data. If the value of the next data point can be extrapolated (within a user-defined margin of error) from previous data points using one of 3 methods, the point is represented by a 2-bit code indicating the method, e.g. quadratic in this case.

Underwood et al. in [25] reports on applying SZ to serial crystallography data from LCLS, where the images consist of floating point values obtained from an integrating detector. In this method, lossless compression is applied to regions of interest consisting of Bragg peaks detected in the image, while binning followed by lossy compression is applied to the rest of the image, with the goal of ensuring that any weak peaks that went undetected will still have their intensities preserved sufficiently well. It is reported that when using this strategy, using SZ for the lossy compression can achieve a compression ratio of 190 while still achieving acceptable data quality, whereas other lossy compression methods tested gave a compression ratio of 35 at best.

## 4 OTHER FORMS OF DATA REDUCTION

The data compression methods discussed thus far work by representing a given file using fewer bits; the original file can be reconstructed from the compressed file (albeit with some inaccuracy in the case of lossy compression). More broadly, though, there are other methods of data reduction which rely on eliminating non-useful data entirely, or transforming the data in a non-recoverable way. These methods have the potential to greatly reduce the amount of data needing to be stored, though of course it is crucial to establish that these methods are reliable before putting them into practice.

### 4.1 Data rejection / vetoing

In some experiments, a large fraction of the data collected does not contain useful information. For example, in experiments at FELs such as serial crystallography and single particle imaging, the sample can consist of a liquid jet containing protein nanocrystals or objects such as viruses passing through the path of the beam. However, only a small fraction of X-ray pulses (in some cases, of order 1%) actually hit a sample to produce an image containing a useful diffraction pattern. So, in these kind of experiments, data volumes can be greatly reduced by rejecting images where the beam did not the target.

A variety of methods have been developed for doing this. In serial crystallography, images where the beam hit a crystal will contain Bragg peaks, whereas miss images will only have scattering from the liquid jet. So, a common approach is to search for Bragg peaks in each image, and only accept images where the total number of peaks exceeds some threshold value; this approach is used in software such as Cheetah [26] and DIALS [27]. Since X-ray diffraction intensity varies with scattering angle, these methods often rely on estimating the background signal in the surrounding area of the image when judging whether a peak is present or not.

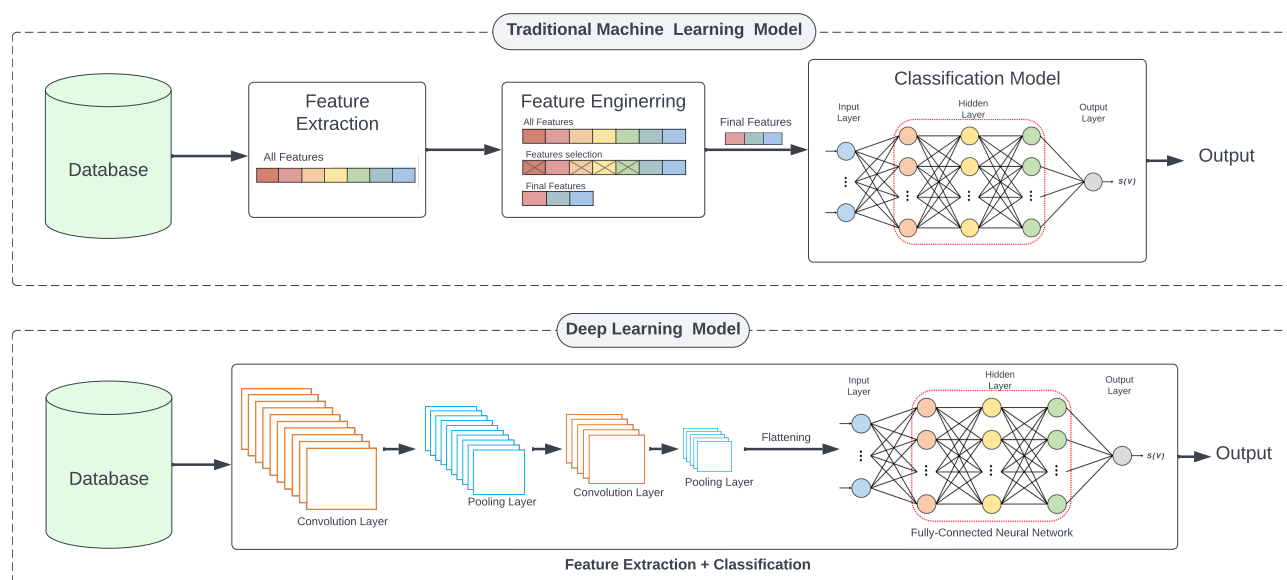


**Figure 6.** Classical Machine Learning and Deep Learning

Machine learning techniques have also been applied to this task, where supervised learning is used to distinguish between good and bad images based on training data from simulation or previous experiments [28, 29, 30, 31]. As illustrated in Fig. 6, there are a variety of methods for doing this; for example, in "traditional" machine learning, features are first extracted from images using algorithms from computer vision, then machine learning is applied to classify images based on these features, whereas in deep learning, the features themselves are also learned using convolutional layers. These methods can potentially be computationally cheaper than peak-counting methods, or require less expert fine-tuning of parameters. However, in some cases a machine learning algorithm trained on one dataset may fail to generalize to others, so it is important for example to validate machine learning methods using different datasets.

## 4.2 Data reduction by processing

Often, the final result of data analysis is much more compact than the original dataset; in determining a protein structure, for example, the data may consist of tens of thousands of diffraction images, while the resulting structure can be described as a list of atomic positions in the molecule.

In some cases the full analysis of a dataset by the user may take months or years, and a lot of this analysis is very experiment-specific, so this is not suitable for achieving fast data reduction close to the detector. Nevertheless, there can be initial processing steps that are common to multiple experiments and which could be applied quickly as part of the DAQ system.

One example of this is azimuthal integration. In some X-ray diffraction experiments, such as powder diffraction, the signal on the detector has rotational symmetry, and so the data can be reduced to a 1-D profile of X-ray intensity as a function of diffraction angle. For a multi-megapixel-sized detector, this corresponds to a factor of 1000 reduction in data size. Hardware-accelerated implementations of azimuthal integration have been developed for GPUs [32], and more recently for FPGAs [33].

### 4.3 Connections between data reduction and on-the-fly analysis

If data reduction involves performing analysis steps on data (e.g. azimuthal integration) or makes the data easier to process (e.g. making the dataset smaller by rejecting bad data) then this synergises with on-the-fly data processing, where the data is processed immediately during the course of the experiment rather than being saved to disk and processed at a later point.

Typically, these sort of data reduction methods have the drawback that if some or all of the original data is discarded, then any errors in the processing cannot be corrected. For example, performing azimuthal integration correctly requires accurate calibration of the centre of the diffraction pattern and any tilt of the detector relative to the beam.

However, since on-the-fly data analysis is useful to users, the trustworthiness of these methods can be established in stages. For example, as a first stage all the raw data may be saved to disk for later analysis, with on-the-fly processing providing quick feedback during the experiment. Once the reliability of the automatic processing is better-established, raw data might only be stored for a shorter time before deletion, to give the opportunity for the user to cross-check for correctness. Finally, once the on-the-fly data processing is fully trusted, it may be possible to only save a small fraction of the raw data for validation purposes.

## 5 HARDWARE-ACCELERATED IMAGE CORRECTION AND DATA REDUCTION

“Off the shelf” data processing hardware of course naturally plays a key role in building data acquisition systems for detectors; even custom hardware such as circuit boards for detector control will incorporate commercial parts such as microcontrollers or FPGAs.

Algorithms can be designed or adapted to take advantage of parallelism on both CPUs and GPUs or pipelining of FPGAs. For instance, algorithms like Fast Fourier Transform (FFT) [34], image processing filters [35], and some statistical calculations [36] can be parallelized effectively. Furthermore, in the realm of data reduction, machine learning models rely significantly on hardware acceleration to address their computational requirements [37, 38, 39].

Here, we give an overview of the distinctive features of CPUs, GPUs and FPGAs for data processing. In particular, a major aspect of high-performance computing is parallelization of work, where a data processing task is divided between many processing units, but how this is achieved varies between devices, which can affect the best choice of hardware for the task.

### 5.1 CPUs - Central Processing Units

The architecture of a typical CPU is shown in Fig. 7. A key feature of modern CPUs is that they’re designed to be able to run many different programs in a way that appears simultaneous to the user. Most modern CPUs are composed of a number of cores; for example, CPUs in the high-end AMD EPYC series have from 32 to 128, though desktop . Each core has a control unit, which is able to independently interpret a series of instructions in software and execute them, along with an arithmetic unit for performing

operations on data, and cache memory for temporarily storing data. Furthermore, CPUs cores can very rapidly switch between executing different tasks, so even a single CPU core can perform many tasks in a way that seems parallel to the user. In most cases, the CPU will be running an operating system, which handles the sharing of resources such as memory and peripherals between the tasks in a convenient way for programmers. High performance computing with CPUs generally involves parallelization of work across multiple cores; in doing this, the different cores can operate relatively independently.

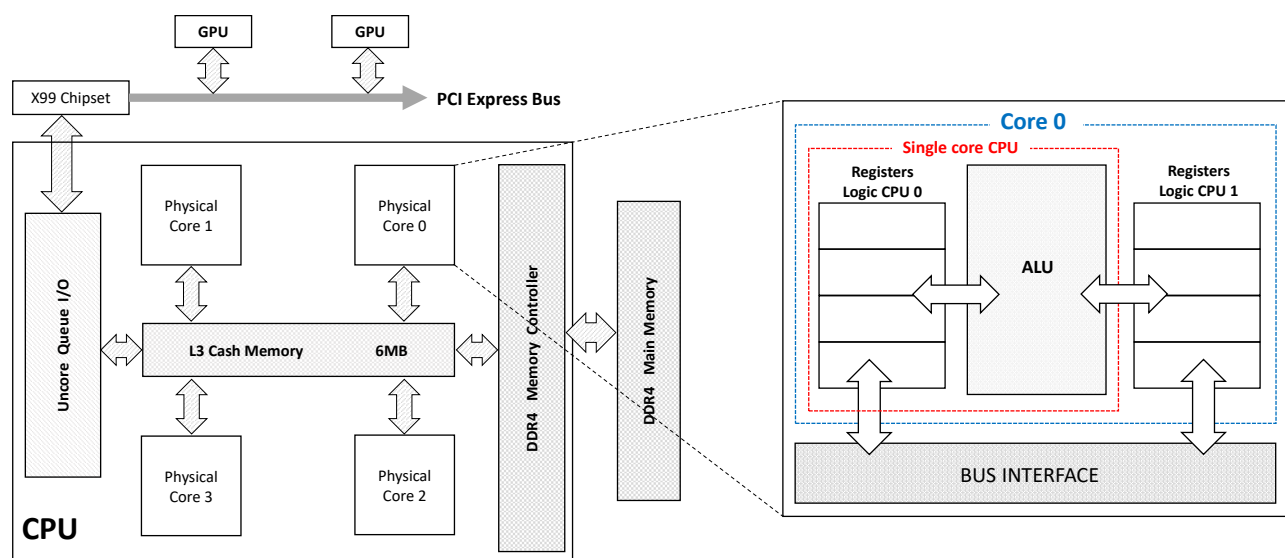


**Figure 7.** Architecture of a Quad-core hyperthreading CPU.

Compared to GPUs and FPGAs, CPUs are generally the easiest to use and program. Indeed, GPUs are virtually always used as accelerator cards as part of a system with a CPU, and it's common for systems based on FPGAs to make use of a CPU (e.g. as part of a System On Chip). In addition, if a task is inherently sequential and cannot be parallelized, then a CPU core may give better performance than a GPU or FPGA. However, CPUs generally have much less parallel processing power than GPUs or FPGAs.

## 5.2 GPUs - Graphics Processing Units

GPUs are designed to allow massively parallel processing for tasks such as graphics processing or general-purpose computing. The basic units of GPUs are called CUDA cores (in NVIDIA GPUs) or stream processors (in AMD GPUs). These are much more numerous than CPU cores, numbering in the thousands, allowing much greater parallelism and processing power. However, rather than each core being able to independently interpret a stream of instructions, these cores are organised into blocks, with all the cores in a block simultaneously executing the same instruction on different data elements - for example, applying the same mathematical operation to different elements in an array. The structure of a typical GPU is shown in Fig. 8.

GPU programming relies on specialized frameworks such as CUDA or OpenCL. GPUs are generally used as accelerator cards in a system with a CPU, and these frameworks firstly allow the CPU to control the GPU's operation (by passing data to and from it, and starting tasks) and secondly to program functions that will run on the GPU. Typically, GPU code contains additional instructions controlling how different GPU cores in a block access data; e.g. when performing an operation on an array, the first core in a block might perform operations on the first element, and so forth. This can be relatively easy to apply to a lot of image

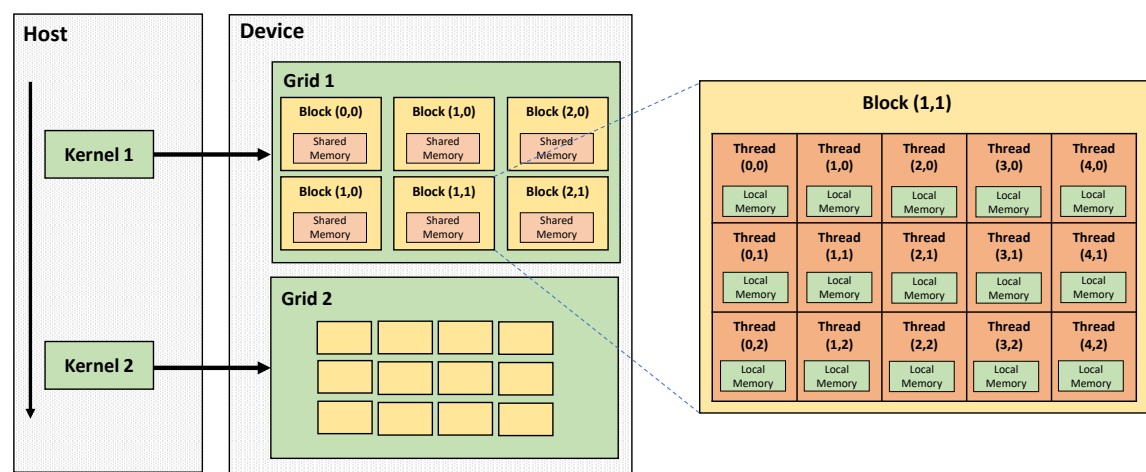


Figure 8. NVIDIA GPU CUDA Block and thread architecture.

366 processing tasks, where each processing step can be applied to pixels relatively independently, but GPU  
367 implementation can be more challenging for some compression algorithms that act sequentially on data.

368 **5.3 FPGAs - Field Programmable Gate Arrays**

369 FPGAs are a type of highly configurable hardware. As shown in Fig. 9, within an FPGA there are many  
370 blocks providing functionality such as combinatorial logic, digital signal processing and memory, with  
371 programmable interconnects between them [40]. While software for a GPU or CPU consists of a series of  
372 instructions for the processor to follow, an FPGA’s firmware configures the programmable interconnects to  
373 produce a circuit providing the required functionality. The large number of blocks in an FPGA can then  
374 provide highly parallel processing and high throughput of data.

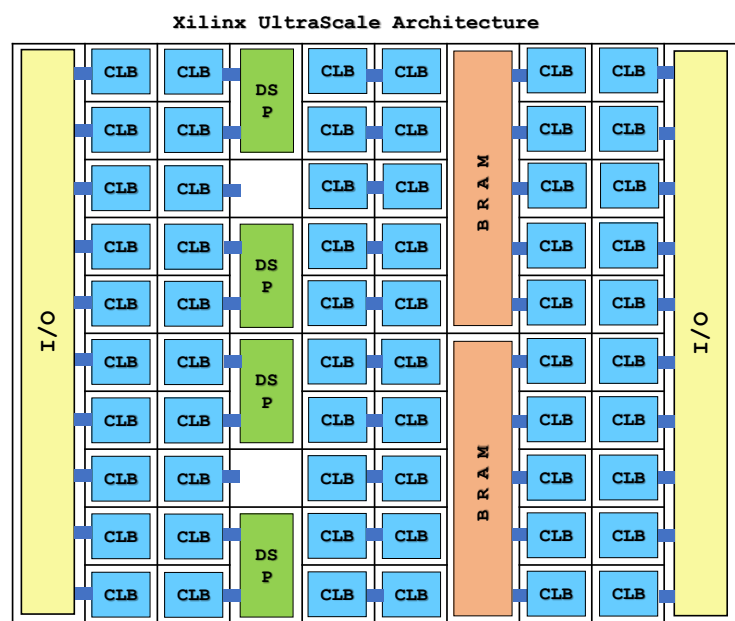


Figure 9. The architecture of the Xilinx UltraScale FPGA accelerator card.



Traditionally, firmware is developed by using a hardware description language to describe the required functionality; a compiler then finds a suitable configuration of blocks and interconnects to achieve this. While hardware description languages differ substantially from conventional programming languages, high-level-synthesis tools for FPGAs have been more recently developed to make it possible to describe an algorithm with a more conventional programming language (such as C++), with special directives in the code being used to indicate how parallelism can be achieved with the FPGA.

A distinctive form of parallelism in FPGAs is pipelining. A series of processing steps will often be implemented as a series of blocks forming a pipeline, with data being passed along from one block to another. This is analogous to a production line in a factory, where each station carries out a particular fabrication step, and goods pass from one station to another. As with the production line, at any given moment there will be multiple data elements in different stages of processing being worked on simultaneously. In turn, to make algorithms run efficiently in an FPGA, they need to be designed to make effective use of this pipeline parallelism. This means that FPGAs tend to be better-suited to algorithms that operate on relatively continuous streams of data, rather than algorithms that rely on holding large amounts of data in memory and accessing them in an arbitrary way. As well as achieving a high throughput, algorithms on FPGA can give a reliably low latency, which can be important in cases where fast feedback is required. However, it is generally more challenging to program FPGAs than CPUs or GPUs.

## 6 DATA TRANSFER AND PROCESSING CHAINS IN DETECTORS

A typical detector and DAQ system consist of series of stages, as illustrated previously in Fig. 1. At each stage, data transfer is needed, and we face a series of bottlenecks which can limit the possible data rate. By doing data reduction earlier on in this chain, the data transfer demands on later stages are reduced, and we can take advantage of this to achieve higher detector speeds. Conversely, the hardware used in earlier stages of this chain is typically more "custom" or specialized, making the implementation of data reduction more challenging, and typically there is also less flexibility in these stages.

The stages in the readout and processing chain are as follows, and the potential for data reduction at each stage will be discussed in more detail in the following section.

- The readout chip (hybrid pixel) or monolithic sensor.
- Readout electronics within the detector itself, which typically incorporate an FPGA, microcontroller or similar.
- Detector-specific data processing hardware. Typically, this consists of one or more PCs, which can include peripherals such as FPGAs or GPUs, but it is also possible to build more specialized systems, such as crates of FPGA boards.
- Generic high-performance-computing hardware, typically in the facility's computing cluster.

### 6.1 On-chip data reduction

The first data bottleneck encountered in the detector is transferring data out of the hybrid pixel readout chip or monolithic sensor. In a pixel detector, we have a 2D array of pixels generating data, and within the chip it's possible to have a high density of signal routing. However, data output takes place across a limited number of transceivers, which are typically located at the periphery of the chip and connect to a circuit board via wire bonds (though there is increasing effort in using Through Silicon Vias - TSVs - for interconnect [41]). In turn, in connecting these to the rest of the readout system, further bottlenecks are

414 faced. To build large detector areas with minimal gaps, it's typical to adopt a modular detector design, with  
415 each module's electronics placed behind it; this naturally creates limits on the space available for PCB  
416 traces and components such as FPGAs and optical transceivers. So, performing data reduction on-chip  
417 could potentially allow the chips to overcome these bottleneck and run at higher speeds.

418 Naturally, any circuitry for on-chip compression must be designed to not occupy excessive amounts of  
419 space in the pixels or periphery. Additionally, readout chips are developed in technology scales that are  
420 relatively large compared to commercial data processing hardware like GPUs and FPGAs, due to the high  
421 cost of smaller nodes. So, rather than implementing general-purpose processing logic into detector chips,  
422 specific algorithms are implemented.

423 Hammer et al. [13] present a design for on-chip data compression for photon counting detectors, using  
424 techniques similar to those discussed previously in Section 3. Firstly, within the pixels, count values are  
425 encoded with a varying step size, with the step size getting larger for larger pixel values such that the step  
426 does not exceed the  $\sqrt{(N)}$  Poisson noise. This is lossy compression, but the additional noise introduced by  
427 this encoding should be less than the Poisson noise. Then, in the chip's periphery during readout, a lossless  
428 compression scheme is applied that applies bit shuffling to the data (much as described for bitshuffle LZ4)  
429 then encodes runs of zeroes efficiently. Applied to example datasets, this computationally-cheap approach  
430 achieved a compression ratio of around 6 for XRD data, compared to 19 obtained with GZIP.

431 One important limitation of on-chip data compression is that in a large tiled detector composed of multiple  
432 chips, the compressibility of the data can vary a great deal between different chips. In X-ray diffraction  
433 experiments in particular, the X-ray intensity close to the beam is much higher than at large scattering  
434 angles, leading to less compression. So, chips close to the beam may encounter data bottlenecks even if a  
435 high overall level of compression is achieved for the detector as a whole.

436 Another example of on-chip reduction is data vetoing by rejecting bad images, as discussed previously.  
437 The Sparkpix-ED chip is one of a family of chips with built-in data reduction being developed by SLAC  
438 [42]. It is an integrating pixel detector with two key features. Firstly, each pixel has built-in memory which  
439 is used to store recent images. Secondly, there is summing circuitry that can add together the signals in  
440 groups of  $3 \times 3$  pixels, to produce a low-resolution image with  $1/9$  of the size. During operation, each  
441 time a new image is acquired the detector will store the full-resolution image in memory and send out the  
442 low-resolution image to the readout system. The readout system will then analyse the low-resolution images  
443 to see if an interesting event occurred (e.g. diffraction from a protein crystal in a serial crystallography  
444 experiment). If so, the detector can be triggered to read out the corresponding full-resolution image from  
445 memory; if not, the image will be discarded. A small prototype has demonstrated reading out low-resolution  
446 images at 1 MHz frame rate, and full-resolution images at 100 kHz.

## 447 6.2 On-detector processing and compression

448 Data processing and compression can potentially be done within the detector, before data is transferred to  
449 the control system (typically over optical links). Once again, this can reduce the bandwidth required for  
450 this data transfer.

451 Typically, on-detector electronics are needed both to control the detector's operation, and to perform  
452 serialization and encoding of data into some standard format so that it can be sent efficiently back to the  
453 control system and received using off-the-shelf hardware. (In some cases, it's also necessary to interface to  
454 additional components such as on-board ADCs.) One particular benefit of serialization is that individual  
455 transceivers on a readout chip typically run at a lower data rate than can be achieved by modern optical

links, so serialization can allow these links to be used more efficiently; for example, even the fastest on-chip transceivers typically do not have data rates above 5 Gbit/s, whereas data sent using 100 Gigabit Ethernet with QSFP28 transceivers consists of 4 channels with a data rate of 25 Gbit/s each. These tasks of control and serialization are typically implemented in an FPGA, or a System-On-Chip (SoC) with an FPGA fabric. So, the most common approach to on-detector data processing is to use the FPGA's processing resources.

As discussed in more detail earlier, FPGAs can provide highly-parallelized data processing, but firmware development can be challenging and time consuming. So, detector-specific processing routines that will always need to be performed on the data are better-suited to FPGA implementation than ones that vary a lot between experiments.

For example, FPGAs in the EIGER photon counting detector perform count-rate correction and image summing [43]. Since the counters in the pixel have a depth of 12 bits, this makes it possible for the detector to acquire images with a depth of up to 32 bits by acquiring a series of images and internally summing them, rather than needing to transfer many 12-bit images to the DAQ system.

One drawback of on-detector processing is that if the FPGA is used for control, serialization and data processing, then it can become more difficult to change the data processing routines. When FPGA firmware is compiled, the compiler will route together blocks in the FPGA to produce the desired functionality. So, changing the data processing routines can change the routing of other functionality in the FPGA, potentially affecting reliability. So, careful re-testing is required after changing the data processing. This is another reason why on-detector processing with FPGAs is mostly used for fixed, detector-specific routines.

### 6.3 Data acquisition hardware such as PCs with accelerator cards

Data sent out from a detector module will normally be received by either one or more DAQ PCs, or more specialized hardware, located either at the beamline or in the facility's computing centre. These parts of the DAQ system can have a range of functions:

- Detector configuration and acquisition control, which requires both monitoring the detector's state and data output, and receiving commands from the control system.
- Ensuring reliable data reception. It is common for a detector's output to be a continuous flow of data, transferred by a simple protocol like UDP without the capability to re-send lost packets [44]. So the DAQ system is required to reliably receive and buffer this data; this typically requires, for example, having dedicated, high performance network or receiver cards.
- Data correction and reduction.
- Transferring data to where it's needed, for example the facility's storage system, online processing and/or a user interface for feedback. This can include tasks like adding metadata and file formatting.

Compared to detectors themselves, these systems tend to be built with relatively off-the-shelf hardware components - for example, standard network cards or accelerator cards. The appeal of using off-the-shelf hardware, in addition to reducing development costs, is that it is easier to upgrade the hardware to take advantage of rapid improvements in technology. These DAQ systems may use conventional CPUs, hardware accelerators such as GPUs and FPGAs, or a mixture of these.

One recent example of this approach is the JungfrauJoch processing system, developed by PSI for the Jungfrau 4-megapixel detector [45]. (A similar approach is taken by the CITIUS detector [46].) The JungfrauJoch system is based on an IBM IC922 server PC, equipped with accelerator cards, and can handle 17 GB/s data when the detector is running at 2 kHz frame rate.

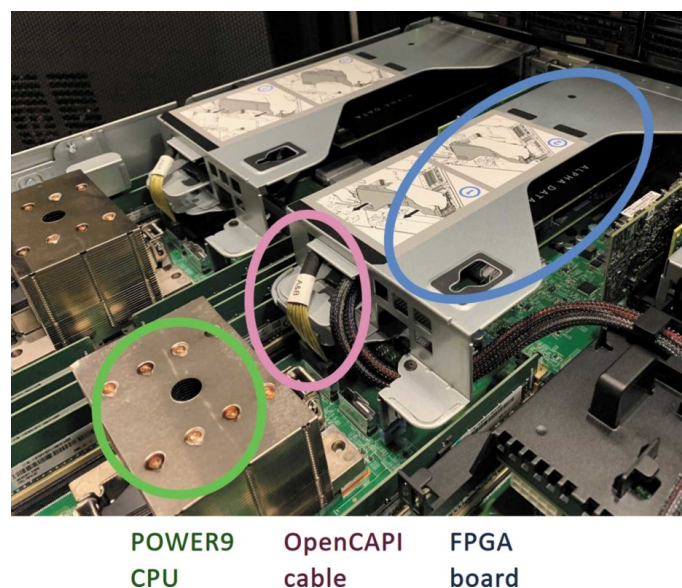


**Figure 10.** A photograph of the IC922 server (IBM) used in JungfrauJoch, showing the FPGA board used for data reception and processing, and the OpenCAPI link allowing coherent access to the CPU's memory. Reproduced from [45] with permission of the International Union of Crystallography.

497 The JungfrauJoch server is shown in Fig. 10 (reproduced from [45] with permission of the International  
 498 Union of Crystallography). Firstly, it is equipped with two "smart network cards" from Alpha Data, each  
 499 with a Xilinx Virtex Ultrascale+ FPGA and a 100 Gigabit Ethernet network link. These receive data directly  
 500 from the detector over UDP. The FPGA then converts the raw data into images, as described in [47].  
 501 Jungfrau is an integrating detector with gain switching, so the raw data consists of ADC values, and the  
 502 process of converting this to either photons or energy values includes subtracting the dark current and  
 503 scaling by an appropriate gain factor. The FPGA also performs the Bitshuffle algorithm, which is the first  
 504 step in Bitshuffle LZ4 compression described previously; since this algorithm involves reordering bits in a  
 505 data stream, this is well-suited to implementation on FPGA. The FPGA is primarily programmed by using  
 506 High Level Synthesis (HLS) based on C++.

507 The data from each FPGA is transferred to the host server PC using OpenCAPI interconnects, which both  
 508 allows high speed data transfer at 25 GB/s, and makes it simpler for the FPGA to access memory on the  
 509 server. The CPU in the server performs the LZ4 part of the Bitshuffle LZ4 lossless compression algorithm,  
 510 then forwards this data to the file system using ZeroMQ so it can be written to the file system as an HDF5  
 511 file. There is also a GPU in the system that can perform tasks such as spot finding in macromolecular  
 512 crystallography, and monitoring aspects of the detector's behaviour such as the dark current. (These tasks  
 513 are well suited to GPUs, since they involve performing operations on full images in parallel.)

514 One promising technological development in this field is that FPGA and GPU vendors are increasingly  
 515 developing accelerator cards with built-in network links for the datacenter market. For example, Xilinx  
 516 have the Alveo line of FPGA cards with two 100 Gigabit Ethernet links and optional high-bandwidth  
 517 memory, and likewise NVIDIA is currently developing GPU cards with network links. So, this will increase  
 518 the availability of powerful, standardized hardware for building DAQ systems.



## 6.4 Computing clusters

Modern light sources are generally supported by large computer clusters for data processing and large storage systems [48]. Data from DAQ PCs or similar hardware at the beamlines can be transferred to them over the facility's network. Data processing in computing clusters can be divided into online analysis, where the data is transferred directly to the cluster to provide fast results to the experiment, and offline analysis where data is read back from storage for processing at a later point. (Naturally, there may not be a sharp dividing line between these two approaches.) In addition to server PCs with CPUs, computing clusters can also incorporate GPUs or less commonly FPGAs.

In a computing cluster, there is generally a scheduling system that controls how tasks are assigned to the computers. This has the advantage of allowing sharing of resources between different experiments and users according to needs, whereas dedicated hardware installed at a beamline may be idle much of the time. Computing clusters are also much better-suited to allowing users to remotely access to their data and providing the software tools required to analyse it. However, this flexibility in task scheduling and usage can make it more difficult to ensure that we can reliably receive and process images from the detector at the required rate; this is one reason for having dedicated DAQ computers at the beamline for receiving detector data.

## 7 CONCLUSIONS

The increasing data rates of detectors for photon science mean there is a strong need for high-speed detector data correction, and data reduction.

There are strong ties between these tasks. On the one hand, data reduction can often yield better results on properly-corrected data, since the correction process can reduce spurious variation in images (e.g. pixel-to-pixel variation in response) and make it easier to exploit redundancy in the data. Conversely, after lossy data reduction it is impossible to perfectly recover the original data, so it is crucial to ensure that the quality of the data correction is as good as possible.

Both of these tasks can benefit from making better use of hardware accelerators such as GPUs and FPGAs for highly parallel processing. The increasing use of accelerators in other areas, such as datacenters, means that we can take advantage of improvements in both their hardware and in tools for programming them. In particular, as FPGAs and GPUs with built-in network links become available "off the shelf", this increases the potential for different labs to build their DAQ systems with compatible hardware, and share the algorithms they develop. Although this paper emphasizes data processing hardware, it is also important to note that well-designed and coded algorithms can deliver much better performance.

Data reduction is a growing field in photon science. To date, lossless compression has mainly been used, since this ensures that there is no loss in data quality, and in some experiments lossless methods can achieve impressive compression ratios. However, lossless compression is relatively ineffective for methods such as imaging, and as data volumes increase there is demand for even greater data reduction in diffraction experiments. So, there will be an increasing need for lossy compression and other methods of reduction. In doing so, it is crucial to use appropriate metrics to test that the data reduction does not significantly reduce the quality of the final analysis. By using well-established methods of lossy compression, for example image compression with JPEG2000, it is easier to incorporate data reduction into existing data analysis pipelines. However, novel methods of data reduction tailored to photon science experiments have the potential for better performance.



Data reduction can be incorporated into different stages of a detector's DAQ chain; generally, performing data reduction earlier in the chain is more challenging and less flexible, but has the advantage of reducing the bandwidth requirements of later stages, and can enable greater detector performance by overcoming bottlenecks in bandwidth. The development of on-chip data reduction is a particularly exciting development for enabling higher-speed detectors, though this would typically require the development of different chips for different classes of experiment. As the demand for data reduction increases, we can expect detectors and experiments to incorporate a series of data reduction steps, beginning with simpler or more generic reduction early in the processing chain, and then more experiment-specific data reduction taking place in computer clusters.

## CONFLICT OF INTEREST STATEMENT

The authors declare that the research was conducted in the absence of any commercial or financial relationships that could be construed as a potential conflict of interest.

## AUTHOR CONTRIBUTIONS

DP: Writing – original draft, review & editing, Conceptualization, Investigation; VR: Writing – review & editing, Visualization; HG: Funding acquisition, Supervision.

## FUNDING

The authors acknowledge support from DESY, a member of the Helmholtz Association HGF. Additional funding for work on data reduction has been provided by multiple sources: LEAPS-INNOV, which has received funding from the European Union's Horizon 2020 research and innovation programme under grant agreement no. 101004728; Helmholtz Innovation Pool project Data-X; and HIR3X - Helmholtz International Laboratory on Reliability, Repetition, Results at the most Advanced X-Ray Sources.

## ACKNOWLEDGMENTS

Thanks to members of the LEAPS consortium and LEAPS-INNOV project, particularly those who have presented and discussed their work on data reduction at events; this has been a valuable source of information in putting together this review. Thanks also to Thorsten Kracht (DESY) for providing feedback on the paper.

## REFERENCES

- [1] Rao R. Synchrotrons face a data deluge. *Physics Today* (2020). doi:10.1063/PT.6.2.20200925a.
- [2] Marras A, Klujev A, Lange S, Laurus T, Pennicard D, Trunk U, et al. Development of CoRDIA: An imaging detector for next-generation photon science X-ray sources. *Nuclear Instruments and Methods in Physics Research Section A: Accelerators, Spectrometers, Detectors and Associated Equipment* **1047** (2023) 167814. doi:https://doi.org/10.1016/j.nima.2022.167814.
- [3] Allahgholi A, Becker J, Bianco L, Delfs A, Dinapoli R, Goettlicher P, et al. AGIPD, a high dynamic range fast detector for the European XFEL. *Journal of Instrumentation* **10** (2015) C01023. doi:10.1088/1748-0221/10/01/C01023.
- [4] Hsieh SS, Iniewski K. Improving paralysis compensation in photon counting detectors. *IEEE Transactions on Medical Imaging* **40** (2021) 3–11. doi:10.1109/TMI.2020.3019461.

- 591 [5] Könnecke M, Akeroyd FA, Bernstein HJ, Brewster AS, Campbell SI, Clausen B, et al. The NeXus data  
592 format. *Journal of Applied Crystallography* **48** (2015) 301–305. doi:10.1107/S1600576714027575.
- 593 [6] [Dataset] The HDF Group. Hierarchical data format version 5 (2000–2010).
- 594 [7] Sayood K. *Lossless compression handbook* (Elsevier) (2002).
- 595 [8] Al-Shaykh OK, Mersereau RM. Lossy compression of noisy images. *IEEE Transactions on Image*  
596 *Processing* **7** (1998) 1641–1652.
- 597 [9] Becker J, Greiffenberg D, Trunk U, Shi X, Dinapoli R, Mozzanica A, et al. The single photon  
598 sensitivity of the Adaptive Gain Integrating Pixel Detector. *Nuclear Instruments and Methods in*  
599 *Physics Research Section A: Accelerators, Spectrometers, Detectors and Associated Equipment* **694**  
600 (2012) 82–90. doi:https://doi.org/10.1016/j.nima.2012.08.008.
- 601 [10] Ballabriga R, Alozy J, Campbell M, Frojdh E, Heijne E, Koenig T, et al. Review of hybrid pixel  
602 detector readout ASICs for spectroscopic X-ray imaging. *Journal of Instrumentation* **11** (2016)  
603 P01007. doi:10.1088/1748-0221/11/01/P01007.
- 604 [11] Broennimann C, Eikenberry EF, Henrich B, Horisberger R, Huelsen G, Pohl E, et al. The PILATUS  
605 1M detector. *Journal of Synchrotron Radiation* **13** (2006) 120–130. doi:10.1107/S0909049505038665.
- 606 [12] Deutsch LP. *DEFLATE Compressed Data Format Specification version 1.3*. No. 1951 in Request for  
607 Comments (RFC Editor) (1996). doi:10.17487/RFC1951.
- 608 [13] Hammer M, Yoshii K, Miceli A. Strategies for on-chip digital data compression for X-ray pixel  
609 detectors. *Journal of Instrumentation* **16** (2021) P01025. doi:10.1088/1748-0221/16/01/P01025.
- 610 [14] Leonarski F, Mozzanica A, Brückner M, Lopez-Cuenca C, Redford S, Sala L, et al. JUNGFRÄU  
611 detector for brighter x-ray sources: Solutions for IT and data science challenges in macromolecular  
612 crystallography. *Structural Dynamics* **7** (2020) 014305. doi:10.1063/1.5143480.
- 613 [15] Gailly J, Adler M. Gzip documentation and sources. *available as gzip-\*.tar in ftp://prep.ai.mit.*  
614 *edu/pub/gnu* (1993).
- 615 [16] Masui K, Amiri M, Connor L, Deng M, Fandino M, Höfer C, et al. A compression scheme for radio  
616 data in high performance computing. *Astronomy and Computing* **12** (2015) 181–190. doi:https://doi.org/10.1016/j.ascom.2015.07.002.
- 617 [17] Ziv J, Lempel A. A universal algorithm for sequential data compression. *IEEE Transactions on*  
618 *information theory* **23** (1977) 337–343.
- 619 [18] Huffman DA. A method for the construction of minimum-redundancy codes. *Proceedings of the IRE*  
620 **40** (1952) 1098–1101.
- 621 [19] Mittone A, Manakov I, Broche L, Jarnias C, Coan P, Bravin A. Characterization of a sCMOS-  
622 based high-resolution imaging system. *Journal of Synchrotron Radiation* **24** (2017) 1226–1236.  
623 doi:10.1107/S160057751701222X.
- 624 [20] Skodras A, Christopoulos C, Ebrahimi T. The JPEG 2000 still image compression standard. *IEEE*  
625 *Signal Processing Magazine* **18** (2001) 36–58. doi:10.1109/79.952804.
- 626 [21] Marone F, Vogel J, Stampanoni M. Impact of lossy compression of X-ray projections onto  
627 reconstructed tomographic slices. *Journal of Synchrotron Radiation* **27** (2020) 1326–1338.  
628 doi:10.1107/S1600577520007353.
- 629 [22] Shensa MJ, et al. The discrete wavelet transform: wedding the a trous and mallat algorithms. *IEEE*  
630 *Transactions on signal processing* **40** (1992) 2464–2482.
- 631 [23] Huang P, Du M, Hammer M, Miceli A, Jacobsen C. Fast digital lossy compression for X-  
632 ray ptychographic data. *Journal of Synchrotron Radiation* **28** (2021) 292–300. doi:10.1107/  
633 S1600577520013326.
- 634

- [24] Di S, Cappello F. Fast error-bounded lossy HPC data compression with SZ. *2016 IEEE International Parallel and Distributed Processing Symposium (IPDPS)* (2016), 730–739. doi:10.1109/IPDPS.2016.11.
- [25] Underwood R, Yoon C, Gok A, Di S, Cappello F. ROIBIN-SZ: Fast and science-preserving compression for serial crystallography (2022). doi:10.48550/arXiv.2206.11297.
- [26] Barty A, Kirian RA, Maia FR, Hantke M, Yoon CH, White TA, et al. Cheetah: software for high-throughput reduction and analysis of serial femtosecond x-ray diffraction data. *Journal of applied crystallography* **47** (2014) 1118–1131.
- [27] Winter G, Waterman DG, Parkhurst JM, Brewster AS, Gildea RJ, Gerstel M, et al. DIALS: implementation and evaluation of a new integration package. *Acta Crystallographica Section D* **74** (2018) 85–97. doi:10.1107/S2059798317017235.
- [28] Rahmani V, Nawaz S, Pennicard D, Setty SPR, Graafsma H. Data reduction for X-ray serial crystallography using machine learning. *Journal of Applied Crystallography* **56** (2023) 200–213. doi:10.1107/S1600576722011748.
- [29] Ke TW, Brewster AS, Yu SX, Ushizima D, Yang C, Sauter NK. A convolutional neural network-based screening tool for X-ray serial crystallography. *Journal of synchrotron radiation* **25** (2018) 655–670.
- [30] Blaj G, Chang CE, Kenney CJ. Ultrafast processing of pixel detector data with machine learning frameworks. *AIP Conference Proceedings* (AIP Publishing) (2019), vol. 2054.
- [31] Chen L, Xu K, Zheng X, Zhu Y, Jing Y. Image distillation based screening for x-ray crystallography diffraction images. *2021 IEEE Intl Conf on Parallel & Distributed Processing with Applications, Big Data & Cloud Computing, Sustainable Computing & Communications, Social Computing & Networking (ISPA/BDCloud/SocialCom/SustainCom)* (IEEE) (2021), 517–521.
- [32] Kieffer J, Wright J. PyFAI: a python library for high performance azimuthal integration on GPU. *Powder Diffraction* **28** (2013) S339–S350. doi:10.1017/S0885715613000924.
- [33] Matěj Z, Skovhede K, Johnsen C, Barczyk A, Weninger C, Salnikov A, et al. Azimuthal integration and crystallographic algorithms on field-programmable gate arrays. *Acta Crystallographica Section A* **77** (2021) C1185. doi:10.1107/S0108767321085263.
- [34] Lin JM. Python non-uniform fast fourier transform (pynufft): An accelerated non-cartesian mri package on a heterogeneous platform (cpu/gpu). *Journal of Imaging* **4** (2018) 51.
- [35] Qasaimeh M, Denolf K, Lo J, Vissers K, Zambreno J, Jones PH. Comparing energy efficiency of cpu, gpu and fpga implementations for vision kernels. *2019 IEEE international conference on embedded software and systems (ICSS)* (IEEE) (2019), 1–8.
- [36] Becker D, Streit A. Real-time signal identification in big data streams bragg-spot localization in photon science. *2015 International Conference on High Performance Computing & Simulation (HPCS)* (IEEE) (2015), 611–616.
- [37] Becker D, Streit A. A neural network based pre-selection of big data in photon science. *2014 IEEE Fourth International Conference on Big Data and Cloud Computing* (IEEE) (2014), 71–76.
- [38] Souza A, Oliveira LB, Hollatz S, Feldman M, Olukotun K, Holton JM, et al. Deepfreak: learning crystallography diffraction patterns with automated machine learning. *arXiv preprint arXiv:1904.11834* (2019).
- [39] Branco S, Ferreira AG, Cabral J. Machine learning in resource-scarce embedded systems, fpgas, and end-devices: A survey. *Electronics* **8** (2019) 1289.
- [40] Abuowaimer Z, Maarouf D, Martin T, Foxcroft J, Gréwal G, Areibi S, et al. Gplace3. 0: Routability-driven analytic placer for ultrascale fpga architectures. *ACM Transactions on Design Automation of Electronic Systems (TODAES)* **23** (2018) 1–33.

- [41] Hügging F, Owtscharenko N, Pohl DL, Wermes N, Ehrmann O, Fritzsche T, et al. Advanced through silicon vias for hybrid pixel detector modules. *Nuclear Instruments and Methods in Physics Research Section A: Accelerators, Spectrometers, Detectors and Associated Equipment* **936** (2019) 642–643. doi:https://doi.org/10.1016/j.nima.2018.08.067. Frontier Detectors for Frontier Physics: 14th Pisa Meeting on Advanced Detectors.
- [42] Rota L, Perez AP, Habib A, Dragone A, Miceli A, Markovic B, et al. X-ray detectors for LCLS-II with real-time information extraction: the SparkPix family (2023). 24th International Workshop On Radiation Imaging Detectors (IWORID 2023), Oslo, Norway.
- [43] Bruckner M, Bergamaschi A, Cartier S, Dinapoli R, Frojdh E, Greiffenberg D, et al. A multiple 10 Gbit Ethernet data transfer system for EIGER (2016). 20th IEEE Real Time Conference, Padova, Italy.
- [44] Gottlicher P, Sheviakov I, Zimmer M. 10G-Ethernet prototyping for 2-D X-Ray detectors at the XFEL. *2009 16th IEEE-NPSS Real Time Conference* (2009), 434–437. doi:10.1109/RTC.2009.5321620.
- [45] Leonarski F, Brückner M, Lopez-Cuenca C, Mozzanica A, Stadler HC, Matěj Z, et al. JungfrauJoch: hardware-accelerated data-acquisition system for kilohertz pixel-array X-ray detectors. *Journal of Synchrotron Radiation* **30** (2023) 227–234. doi:10.1107/S1600577522010268.
- [46] Grimes M, Pauwels K, Schüllli TU, Martin T, Fajardo P, Douissard PA, et al. Bragg coherent diffraction imaging with the CITIUS charge-integrating detector. *Journal of Applied Crystallography* **56** (2023) 1032–1037. doi:10.1107/S1600576723004314.
- [47] Redford S, Andrä M, Barten R, Bergamaschi A, Brückner M, Dinapoli R, et al. First full dynamic range calibration of the JUNGFRAU photon detector. *Journal of Instrumentation* **13** (2018) C01027. doi:10.1088/1748-0221/13/01/C01027.
- [48] Thayer J, Damiani D, Ford C, Dubrovin M, Gaponenko I, O’Grady CP, et al. Data systems for the Linac Coherent Light Source. *Advanced Structural and Chemical Imaging* **3** (2017) 3. doi:10.1186/s40679-016-0037-7.

## FIGURE CAPTIONS